Proceedings of the ASME 2015 34th International Conference on Ocean, Offshore and Arctic Engineering
OMAE2015
May 31-June 5, 2015, St. John's, Newfoundland, Canada

OMAE2015-41732

COMPARISON OF EXPERIMENTAL DATA OF A MOORED MULTIBODY WAVE ENERGY DEVICE WITH A HYBRID CFD AND BIEM NUMERICAL ANALYSIS FRAMEWORK

Ali Nematbakhsh
Centre for Ships and Ocean Structures (CeSOS)
Norwegian University of Science and Technology
Trondheim, Norway, 7491
Email: ali.nematbakhsh@ntnu.no

Constantine Michailides
Centre for Ships and Ocean Structures (CeSOS)
Norwegian University of Science and Technology
Trondheim, Norway, 7491
Email: constantine.michailides@ntnu.no

Zhen Gao
Centre for Autonomous Marine Operations and Systems (AMOS) and Centre for Ships and Ocean Structures (CeSOS)
Norwegian University of Science and Technology
Trondheim, Norway, 7491
Email: zhen.gao@ntnu.no

Torgeir Moan
Centre for Autonomous Marine Operations and Systems (AMOS) and Centre for Ships and Ocean Structures (CeSOS)
Norwegian University of Science and Technology
Trondheim, Norway, 7491
Email: torgeir.moan@ntnu.no

ABSTRACT
In the present paper, a hybrid Computational Fluid Dynamics (CFD) and Boundary Integral Element Method (BIEM) framework is developed in order to study the response of a moored Multibody wave Energy Device (MED) to a panchromatic sea state. The relevant results are the surge and heave responses of the MED. The Numerical Analysis Framework (NAF) includes two different models; the first model uses Navier-Stokes equations to describe the flow field and is solved with an in-house CFD code to quantify the viscous damping effect, while the second model uses boundary-integral equation method and is solved with the tool WAMIT\SIMO\RIFLEX. By studying the free decay tests with the Navier-Stokes based model, the uncoupled linear and quadratic damping coefficients of the MED in surge and heave directions are calculated. These coefficients are given as input to the WAMIT\SIMO\RIFLEX model and the responses of the MED to different wave conditions are determined. These responses are compared with the experimental data and very good agreement is obtained. The MED responses calculated by the presented NAF have been obtained in connection with a hydrodynamic modeling competition and selected as one of the numerical models, which well predict the blind experimental data that were unknown to the authors.

KEYWORDS: Surface piercing floater, computational fluid dynamics, multibody energy device, wave energy converters, quadratic damping.

ABBREVIATIONS
BIEM	Boundary Integral Element Method
CFD	Computational Fluid Dynamics
MED	Multibody Energy Device
NAF	Numerical Analysis Framework
SHCPC	Submerged Horizontal Cylinder with domed ends and rectangular shaped surface Piercing Columns
WEC	Wave Energy Converter

INTRODUCTION
In offshore engineering, it is common to determine wave loads by using potential flow solver; this linear analysis is frequently applied due to low computational cost allowing investigation of different parameters (e.g. frequency, wave direction, metacentric height, etc.) within short time. Relevant viscous effects are included by distributed drag type load. On the other hand, Computational Fluid Dynamics (CFD) is a computer-based simulation of a fluid flow, modelled by solving a set of field equations describing the dynamics of the fluid flow and

finds a lot of applications in the offshore engineering science. The main advantage of the CFD analysis is the high fidelity accuracy of the calculated response quantities as well as the better representation of the physical problem and consequently capturing of possible non-linear phenomena.

The potential theory is a reliable approach to simulate offshore structures when the structure motion is linear and the natural frequencies of the structure are far from the ocean waves peak frequency. In these cases, the assumption of linear motions and rough estimation of the hydrodynamic damping coefficients do not greatly affect the accuracy of the results. However, in some types of offshore structures such as Wave Energy Converters (WECs) the design purpose is to maximize the structure's motion in order to harvest the maximum power. In these cases, using CFD methods leads to more reliable results, although they require a considerable computational cost. Some examples of CFD based models, used for WEC simulations, are described in the following. Agamloh et al. [1] used a CFD tool to model an existing prototype of a heaving buoy WEC. They used a cylinder shape structure as a simplified model for the WEC. They stated that even though the simplified model gives reasonable results, the precise modelling requires more sophisticated CFD tools and demands more computational resources. Bhinder et al. [2] studied a surging WEC and evaluated different CFD commercial softwares concluded that the softwares in which re-meshing techniques are not required, can lead to a considerable lower computational cost. Westphalen et al. [3] also used various CFD tools to study a bobber WEC and pointed that good agreement between the numerical models with experimental data can be achieved by using CFD approach. In all these works the main conclusion is that CFD method is a robust and reliable approach to model WECs but requires a considerable computational time. This drawback of the CFD methods limits its applications to short time simulations and prevent the application for real ocean wave conditions in which around 30 minutes real time simulation is required for only one sea state.

On the other hand engineering design of all possible kind of WECs is based on linear potential theory as have been developed by Falnes and Budal [4], Mei and Newman [5], Falnes [6,7,8], Payne et al. [9], Gomes et al. [10] and Michailides and Angelides [11,12]. For the analysis of WECs usually the viscous effects are represented by distributed drag type loads (Muliawan et al. [13,14,15], Michailides et al. [16,17]) and are included in the analysis process according to design regulations (DNV [18]). The efficiency of the aforementioned method is usually validated against experimental model tests.

In order to determine the MED response to ocean waves in reasonable time and have an accurate prediction for the MED responses at the ocean wave frequencies which coincide with the MED's natural frequencies, a hybrid CFD and BIEM framework is developed and presented in this paper. In this hybrid approach the damping coefficients are determined by using CFD methods and given as an input to the BIEM based model. The CFD model is based on a in-house code developed by Nematbkahsh et al. [19] to model offshore structures in interaction with waves. The developed CFD model is capable of capturing nonlinear hydrodynamic effects. The model was successfully used to study wave responses of different types of floating wind turbines [20,21]. The BIEM model is solved with the well validated tool WAMIT\SIMO\RIFLEX. Using this approach will significantly increase the accuracy of the BIEM based model while keeps the computational cost reasonable.

The developed NAF participated to OMAE hydrodynamic modeling competition for a MED device. Initially the competition organizer, Center for Ocean Energy Research (COER) in Maynooth University, gave to the competitors: (a) the geometry of the wetted surface of the model (*.igs file format), (b) a brief description of the mooring lines, (c) a time series of the surface elevation of the incoming waves, and (d) a reference paper for the MED device [22]. The competition criteria are based on a comparison of the surge and heave motions of a surface piercing body of the MED against the experimental data in a blind way. The current hybrid framework was selected by COER as one of the accurate numerical models when compared with the blind experimental data. This competition is sponsored by ASME 2015 Ocean, Offshore and Arctic Engineering Conference OMAE 2015.

NUMERICAL ANALYSIS FRAMEWORK

The physical problem under investigation coincides with a Multibody Energy Device (MED) that has a generic geometry. However, considering the MED's natural frequencies it is more likely to have application as a WEC. The MED consists of two rigid bodies; the first rigid body is a Submerged Horizontal Cylinder with domed ends and rectangular shaped surface Piercing Columns (SHCPC). The second body is a fully submerged clump mass. In Figure 1 the physical model of the MED is presented as built for the experimental investigation of the behavior of the MED in interaction with different wave conditions [22].

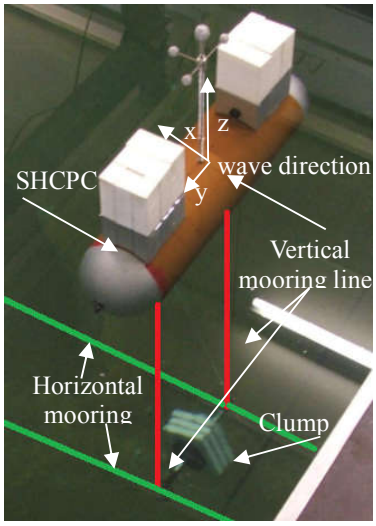

Fig. 1: Physical model of the MED in wave flume [22]

The two rigid bodies are connected with two vertical mooring lines. The volume displacement of the SHCPC is 3.034 times larger than the required displacement volume for SHCPC to remain neutrally buoyant. As a consequence, in calm water the vertical mooring lines are in tension. In order to keep MED in position, horizontal mooring lines are used. The horizontal mooring lines provide horizontal and heave stiffness to the MED. Also, the horizontal mooring lines allow the submerged clump mass to move only in the heave direction. In Table 1 basic geometry characteristics of the MED are tabulated. The numerical analysis was performed at model scale using the actual properties of the test model and as a result there are no scaling effects. The tests were undertaken at the Kelvin Hydrodynamics Laboratory in the University of Strathclyde, Glasgow, UK. The tank depth was 2.2 m, tank length 76 m, tank width 4.6 m and the distance from the model to the wavemaker was 37 m. Further details as far as the MED properties can be found in [22].

The NAF consists of: (a) an appropriate 3D CFD model for the decay tests of the MED (b) an appropriate 3D multibody structural model (based on BIEM results) for the calculation of the responses of SHCPC and (c) a numerical analysis process for the calculation of the SHCPC linear and quadratic damping coefficients in surge and heave directions, based on the results from decay tests of the 3D CFD model. An outline of the NAF, developed and applied in the present paper, is presented in Figure 2. In the following subsections, the components of the numerical analysis framework are briefly described.

Table 1. Design characteristics of the MED

Property	Value
Cylinder diameter [m]	0.2
Length of cylindrical surface [m]	0.6
Overal length of submerged cylinder [m]	0.8
Submergence of centerline of cylinder [m]	0.2
Rectangular's dimensions of piercing columns [m×m]	0.112×0.15
Displacement of SHCPC [m^3]	0.027
Structural mass of SHCPC [kg]	8.9
Weight of clump mass [kg]	19.75
Length of each vertical mooring line [m]	1.3
Tension of each vertical mooring line [N]	88.35
Horizontal mooring lines; heave stiffness [N/m]	36.30
Horizontal mooring lines; surge stiffness [N/m]	129.1

3D CFD model

A CFD model is used to determine the damping coefficients of SHCPC by performing free decay tests. The model is based on solving the Navier-Stokes equations in time along with free surface modelling to capture the free surface position and an immersed boundary method to track the solid (SHCPC here).

The Navier-Stokes equations which are supplemented by the mass conservation equation can be written as the following.

$$\rho\left(\frac{\partial \mathbf{V}}{\partial t}+\nabla\cdot\left(\mathbf{VV}\right)\right)=-\nabla p+\nabla\cdot\mu\left(\nabla\mathbf{V}+\nabla\mathbf{V}^{T}\right)+\rho\mathbf{g}+\mathbf{F} \quad (1)$$

$$\nabla\cdot\mathbf{V}=0 \quad (2)$$

where ρ is density, **V** is velocity, p is pressure, μ is dynamic viscosity and **g** is the gravity. These two equations are the standard equations for the incompressible fluids. Only a force term, **F**, is added to the right hand side of Equation 1. This term represents the presence of the solid (SHCPC here) in the numerical domain.

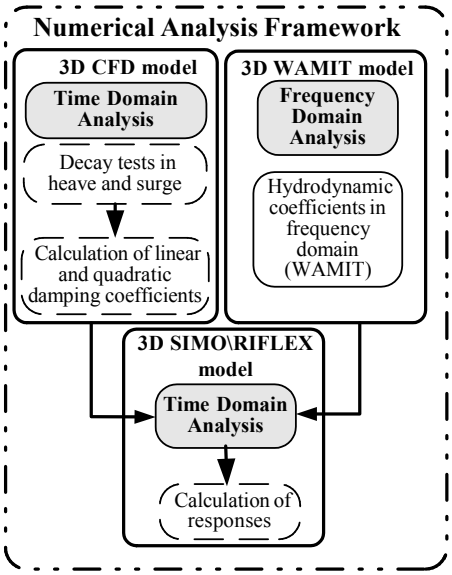

Fig. 2: Outline of the generic NAF

The Navier-Stokes equations are solved in the whole numerical domain by second order finite volume discretization techniques in space and time. The updated velocities, calculated from the Navier-Stokes equations, are used to update the free surface position. Free surface position is in fact the water-air interface and one of the standard CFD methods to track the two-phase flows' interface can be used. In here, level set method [23], which is a suitable approach to model two-phase flows with high density ratio (1000:1 here), is used. After updating the free surface position, the SHCPC position needs to be updated. In order to update the SHCPC position immersed boundary method [24] is used. Immersed boundary method is a standard approach to study solid-fluid interaction problems. In this method the solid is immersed in the numerical cells, therefore no re-meshing technique is required. In this method, initially the whole numerical cells, including the cells occupied by the solid, is assumed as fluid and the Navier-Stokes equations are solved for them. Then, additional constraints due to the presence of the solid are imposed to the solid cells. Finally, the updated position of the SHCPC is calculated based on integration of the hydrodynamic and external loads on the SHCPC.

The hydrodynamic loads can be determined directly from the Navier-Stokes solver. The external loads here are only the two tendon forces. While for the SHCPC the hydrodynamic and hydrostatic effects are fully considered, regarding the clump mass only the hydrostatic effect is taken in to account. Since the ballast is relatively small in volume and far from the free surface and SHCPC, neglecting the hydrodynamic effects should not highly affect the SHCPC motion.

The numerical model is solved on a structured grid shown in Figure 3. Slip boundary condition is imposed on all sides of the numerical domain and no penetration boundary condition is imposed on the solid-fluid interface.

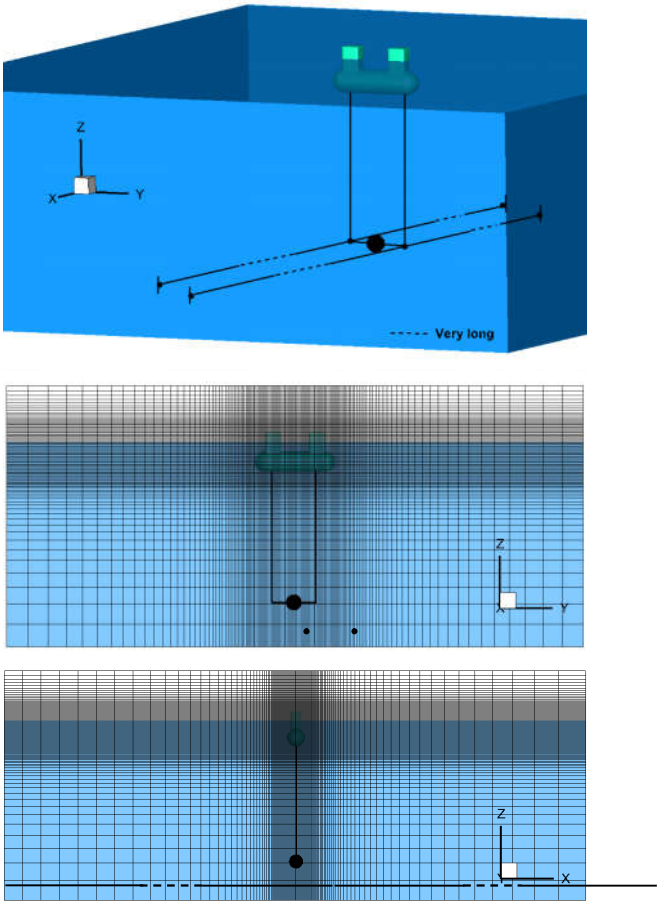

Fig. 3: CFD numerical domain and the structural grid points used to discretize the domain in the CFD model. 115×140×95 in x, y and z directions are used for the simulations.

3D WAMIT\SIMO\RIFLEX model

In the present paper a time-domain global model for the estimation of the response of the MED is developed and used. The complete numerical model of the MED was developed in the coupled analysis tool, WAMIT\SIMO\RIFLEX. This tool further extends the capabilities of the WAMIT [25] SIMO [26] and RIFLEX [27] tools.

Initially a panel model of the wet surface of the SHCPC is developed according to the geometry details that have been provided by COER. Then hydrodynamic analysis of the panel model is performed with WAMIT in order to calculate the hydrodynamic coefficients of added mass, radiation potential damping, hydrostatic stiffness and excitation forces in frequency domain. The hydrodynamic coefficients are estimated using panel method and are based on potential theory. The hydrodynamic coefficients that are used for the time domain analysis are presented in Figure 4; there exist very good agreement compared to the hydrodynamic coefficients that are presented in [22]. It must be noted that initially a convergence study was performed in order to define the size of the panels of the panel model of the SHCPC.

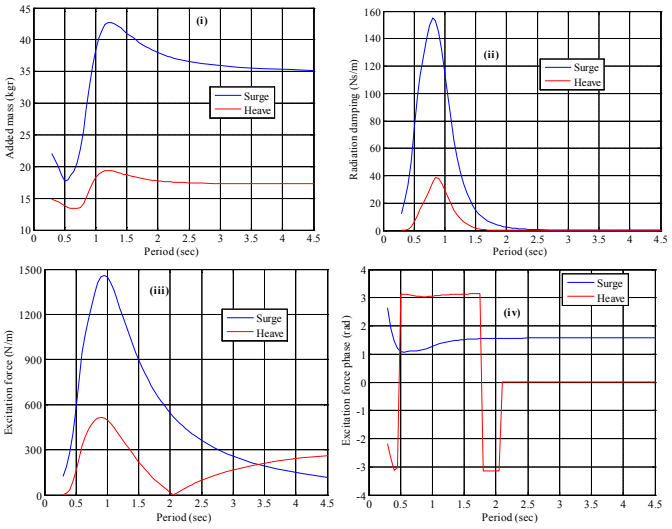

Fig. 4: Hydrodynamic coefficients of added mass (Fig. 4i), radiation damping (Fig. 4ii), excitation forces (Fig. 4iii) and phase of excitation forces (Fig. 4iv) of the wet surface of the SHCPC for surge and heave

SIMO is then used in order to model the hydrodynamic loads on rigid-body SHCPC in time-domain, including the first-order and second-order wave loads. RIFLEX is a nonlinear time domain program with a finite element formulation that can handle large displacement and rotations. RIFLEX also has the capability of performing a coupled analysis, where one or more rigid-body floating structures are integrated with a dynamic model of mooring lines and arbitrary coupling forces in the time domain. With RIFLEX and through flexible beam elements, the simulation of mooring lines is achieved. The structural model of the MED is dealt within RIFLEX and the equation of motion is solved in the time domain in RIFLEX with the following Equation:

$$R^I\left(r,\ddot{r},t\right)+R^D\left(r,\dot{r},t\right)+R^S\left(r,t\right)=R^E\left(r,\dot{r},t\right) \quad (3)$$

where $\mathbf{R}^{\mathrm{I}}$ is the inertia force vector, $\mathbf{R}^{\mathrm{D}}$ is the damping force vector, $\mathbf{R}^{\mathrm{S}}$ is the internal structural reaction force vector, $\mathbf{R}^{\mathrm{E}}$ is

the external force vector and $\mathbf{r}, \dot{\mathbf{r}}, \ddot{\mathbf{r}}$ are the structural displacement, velocity and accelerations vectors. It should be noted that all the force vectors are established by assembly of the element distributions and the specified discrete nodal forces. Equation 3 expresses a nonlinear system of differential equations due to displacement dependencies in the inertia and the damping forces between the external load vector and the structural displacement and velocity.

The WAMIT\SIMO\RIFLEX model of the MED (Fig 5) is a multibody model consisting of two different rigid bodies that can undergo three translational motions and three rotational motions as well, and of vertical and horizontal mooring lines that are modeled through beam elements. It must be noted that the fairleads in Fig. 5 are artificial (dummy) elements in order the vertical mooring lines to be rigidly connected with the rigid bodies SHCPC and clump mass.

The first rigid body is the SHCPC. Hydrodynamic coefficients of SHCPC (Fig 4) are calculated based on the potential theory approach. The second rigid body is the clump mass and is modeled as a point mass without considering any kind of hydrodynamic coefficients. Also, the hydrodynamic interaction between the two rigid bodies is not modeled in the present study. The horizontal mooring lines allows the clump mass to move only in the heave direction. The linear and the quadratic damping coefficients, calculated with the process described in the next sub-section, are given as input to the $\mathbf{R}^D$ vector (Eq. 3)

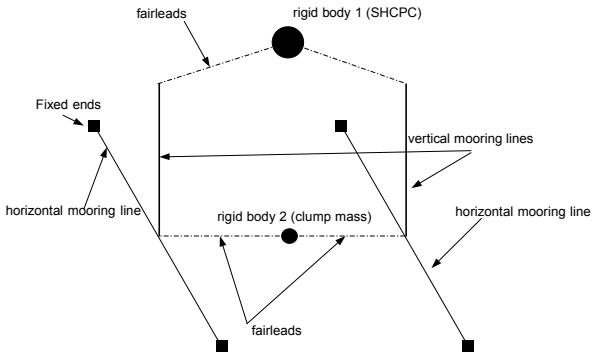

Fig. 5: Sketch of the numerical model in WAMIT\SIMO\RIFLEX

Damping Coefficient Calculation

In the decay test, the SHCPC motion in a specific degree of freedom can be written as the following [28]:

$$\ddot{x}_i + p_i \dot{x}_i + q_i \dot{x}_i |\dot{x}_i| + r_i x_i = 0 \qquad (4)$$

where p_i is the linear damping, q_i is the quadratic damping, r_i is the restoring stiffness and term and x_i is the displacement in the i direction.

Equation 4 is a nonlinear differential equation. In order to solve this equation, the quadratic term $(q_i \dot{x}_i |\dot{x}_i|)$ can be replaced by an equivalent linear damping term and the following formula can be obtained to derive the damping coefficients [28].

$$\frac{2}{T_i} \ln\left(\frac{X_{i_n}}{X_{i_{n+1}}}\right) = p_i + X_{i_{n+\frac{1}{2}}} \frac{16}{3T_i} q_i \qquad (5)$$

In Equaion 5, T_i is the response period, X_{in} is the response amplitude in the n^{th} oscillation. When we assume p_i and q_i are constant, it implies that the damping coefficients are independent of oscillation amplitude. The accuracy of this assumption can be checked by studying decay tests with different initial displacements. Equation 5 can be derived by using a standard method for solving linear equations and by assuming that $\left(2\pi/\ln(X_{i_n}/X_{i_{n+1}})\right)^2 >> 1$ is much larger than one. This assumption is almost always a reasonable approximation.

Also by performing decay tests, damping coefficients are calculated at the floater natural frequencies, but it might be different in other frequencies. However, the damping terms are important when the structure is responding to wave frequencies close to the floater natural frequencies. Therefore small variation of damping coefficients outside the floater natural frequencies should not highly affect the general wave response of the floater.

Different methods can be used to determine the damping coefficients. The first and probably the best one is to setup experimental decay tests and determine the damping coefficients. The only issue regarding experimental tests is the Reynolds scaling problem. Scaling the prototype according to the Froude number usually will not keep the Reynolds number the same. If the damping coefficients be function of Reynlods number, the damping coefficients determined from the scale model experiments are not very trustable.

The second option is to perform decay tests by using potential theory based numerical model. In this case, the potential theory will predict the radiation damping of the floater and the viscous damping should be estimated from some reference manuals. In the reference manuals, the approximate viscous damping coefficients for simple floating structures are available. The damping coefficients for more complex structures can be determined by using distributed damping coefficients. In this case, the structure is divided to simpler sections and proper viscous damping coefficients will be assigned to each section. Using distributed damping coefficients may have low accuracy at the section joints.

The third option is to use CFD techniques. This method can give very good estimation of damping coefficients, but it comes with considerable computational cost. The damping computed form CFD models, the same as experimental tests, includes both radiation and viscous dampings. CFD methods can be used for both full-scale and scale-model prototypes with not considerable difference in the computational cost. In the current research, the CFD method is used to determine the damping coefficients by performing decay tests in surge and heave directions with different initial displacements.

RESULTS AND DISCUSSION

Decay test and regular wave results

MED free decay tests are performed by the CFD method to determine the damping coefficients. The results will be uncoupled damping coefficients in surge and heave directions. The damping coefficients calculated by the CFD methods include both radiation and viscous damping. In Figure 6 and 7 surge and heave decay tests are presented.

The decay tests are performed for different initial displacements to study if the damping coefficients are function of oscillation amplitude. Using equation 5 to compute the linear and quadratic damping shows that the linear damping does not considerably vary with respect to the initial displacements, while the quadratic damping shows dependency to the initial displacement for both surge and heave decay tests. The linear damping obtained in the surge direction agrees well with the experimental data provided, but the heave decay tests shows higher damping in comparison with the experimental data [22]. We noticed a same trend in the CFD heave decay simulation of a tension leg platform modeled earlier and it seems that the damping in heave direction is very sensitive to the grid resolution. A correction factor is used based on the previous CFD studies on different grid resolution. The simulations with finer grid points for CFD decay tests are under development.

The MED natural frequencies predicted by the CFD method in surge and heave directions are 4.24 seconds and 2.16 second which is 13 percent and 8 percent different from the values predicted by the potential theory. Different structural models in these two approaches may explain the difference.

Although CFD models for long time panchromatic sea state are desirable, it takes extremely long time for simulation. Therefore, BIEM method will be used to study the interaction of MED with various wave conditions with the provided damping coefficients from the CFD method with some tunings based on the MED RAO responses provided in reference [22]. Finally the surge linear and quadratic damping equal to 2.86 and 36.1 Nsec/m and heave linear and quadratic damping equal to 2.75 and 10.1 Nsec/m, are used as the uncoupled damping values in 3D\WAMIT\SIMO\RIFLEX model.

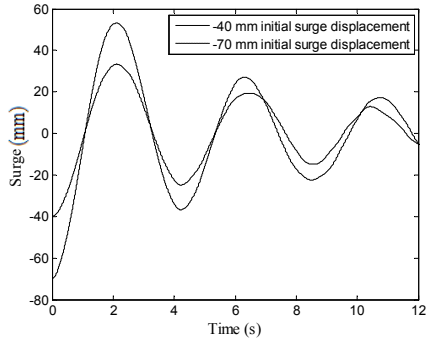

Fig. 6: Surge decay tests for two initial displacements based on the CFD model

In Figures 8 and 9 comparisons of surge and heave RAO of the SHCPC are presented.

The comparisons are performed between the results, derived through the application of the present NAF against corresponding experimental data [22]. The comparisons are performed for different wave amplitudes, namely 12 mm, 25 mm and 75 mm. It can be seen that there is a very good agreement for both examined motions, surge and heave, of the SHCPC and for all the examined wave amplitudes.

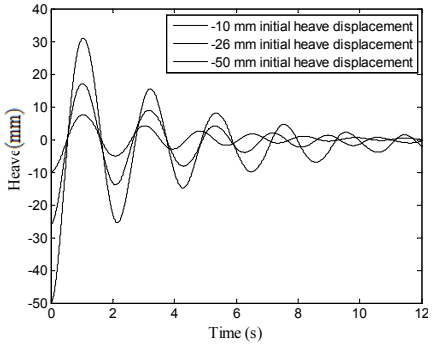

Fig. 7: Heave decay tests for three initial displacements based on the CFD model

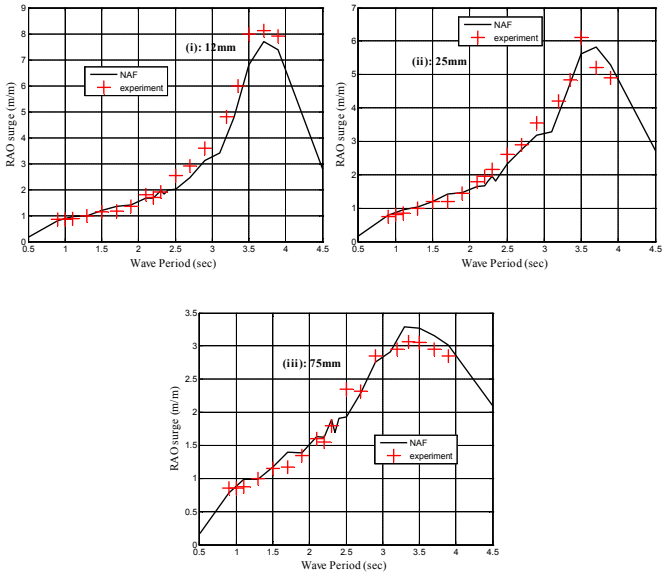

Fig. 8: Comparison of surge RAO for wave amplitude 12 mm (Fig. 8i), 25 mm (Fig. 8ii) and 75 mm (Fig. 8iii), against experimental data [22].

Also, it can be seen that heave natural period is 2.35 sec while surge natural period is 3.70 sec. It should be stressed that the values that the RAOs have at the resonance regions for different wave amplitude for both examined motions indicates the SHCPC nonlinear response.

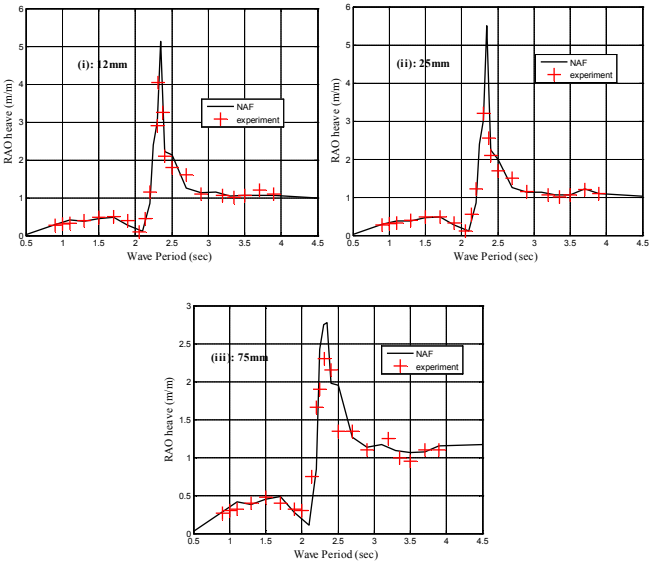

Fig. 9: Comparison of heave RAO for wave amplitude 12 mm (Fig. 9i), 25 mm (Fig. 9ii) and 75 mm (Fig. 9iii), against experimental data [22].

Irregular wave results

As explained in the Introduction section, COER provided a data set of the time series of the surface elevation of the incoming waves as measured by a wave gauge in a specific position during the experiments. The specific data set describes a panchromatic sea state. In Figure 10 the spectrum and corresponding time series of the wave elevation of the panchromatic sea state are presented. The time step of the provided time series is equal to 0.00729 sec and the overall duration is 512.89524 sec. The maximum wave elevation is 97.05 mm, the minimum wave elevation is 82.99 mm and the standard deviation of the time series is 23.38 mm. The wave direction coincides with the x axis (Fig. 1). According to the calculated spectrum of the panchromatic sea state, it is expected that both surge and heave motions of SHCPC will be in their resonance regions. Below responses as calculated from NAF for the aforementioned wave elevation are presented. It must be noted that the experimental data responses are sent from COER after the completion of the competition. The time step that was used in the numerical analysis for both wave elevation and calculation of the responses was 0.00729 sec. In Figures 11 and 12, a comparison of the surge and heave motions of SHCPC as calculated from the NAF against recorded experimental data time series are presented.

In Figures 11i, 11ii, 12i and 12ii, there exist two lines for the motions as calculated from the NAF. The black curve corresponds to the results calculated from NAF with wave elevation insert position at X=-1.7 and Y=0, while the blue curve corresponds to the results with wave elevation insert position at X=0 and Y=1.7. Due to a misunderstanding of the wave elevation position, the time histories of the motions that have been sent for evaluation to COER are depicted with the dot black line (NAF X=-1.7 Y=0). It can be seen in Figures 11ii

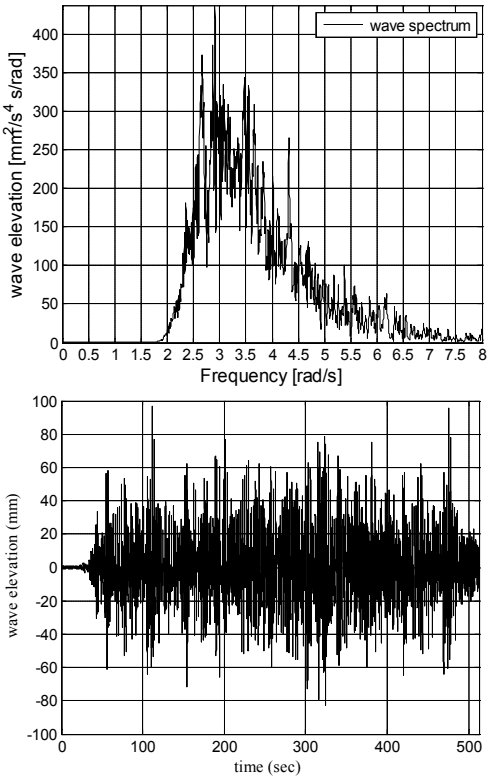

Fig. 10: Spectrum and time series of wave elevation of the panchromatic sea state

and 12ii that surge and heave curves (NAF X=-1.7 Y=0) are in different phase (0.5 sec) compared to the experimental data. This is due to 1.7 meter difference in the assumed wave gauge position in the numerical analysis with the wave gauge position of the experimental data. For both motions it can be seen that there is a very good agreement between the experimental data (COER) and the numerical results of NAF (NAF X=0 Y=1.7). The differences in the peak maximum and minimum values indicate that the damping model that was calculated with the CFD 3D model can be further optimized (e.g. finer grid in the CFD numerical model). As far as statistical analysis of the time histories of surge and heave motions, in Table 2 comparisons of numerical and experimental statistical quantities are presented. There is good agreement in mean and standard deviation of the experimental and numerical data. The kurtosis values close to three and very small Skewness show nearly Gaussian distribution of surge and heave. In Figure 13 comparisons of surge and heave spectra for the panchromatic sea state are presented. It can be seen that there is a good agreement between the experimental and numerical spectra. For surge motion, the NAF spectrum shows slightly higher values probably due to uncertainties of the estimated damping coefficients. Regarding the heave motion there is a very good agreement in the values, while there is a slight shifting in the peak frequency probably due to the structural modeling.

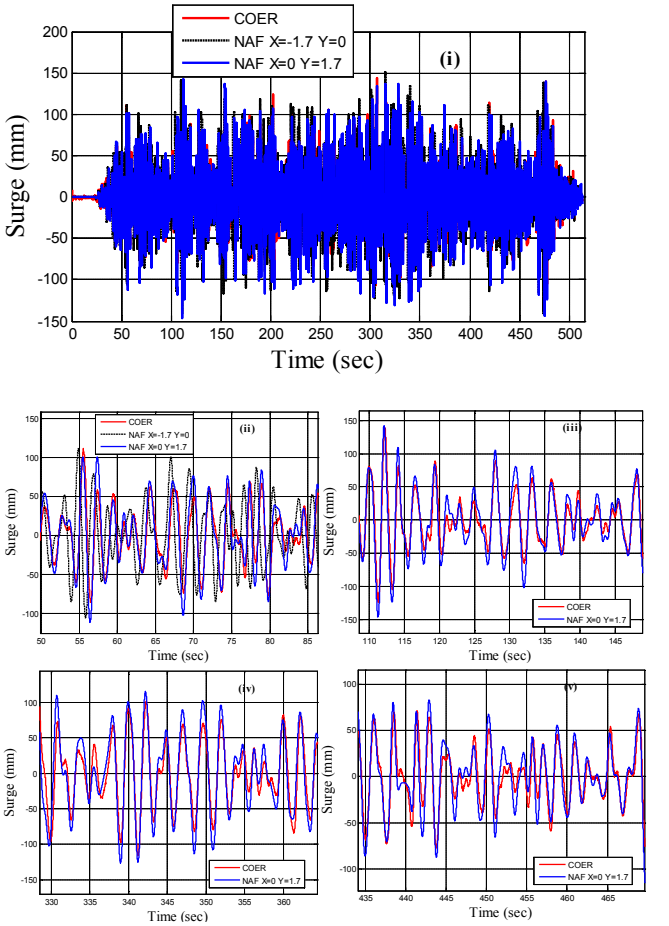

Fig. 11: Comparison of surge motion of SHCPC for the test panchromatic sea state

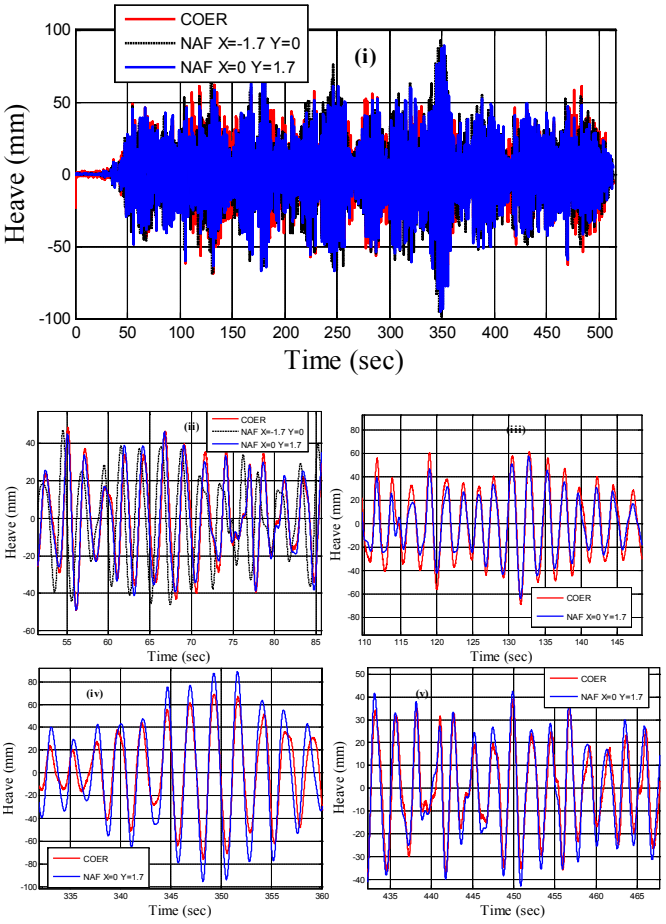

Fig. 12: Comparison of heave motion of SHCPC for the test panchromatic sea state

With the present NAF and apart from the calculation of the heave and surge motions of the SHCPC, other response quantities can be calculated (e.g. mooring line tension forces, pitch of SHCPC, motions of the clump mass). In Figure 14 time series of pitch motion of SHCPC (Fig. 14i) and tension of one vertical mooring line (Fig. 14ii) for the examined panchromatic sea state are presented. The maximum pitch motion of the SHCPC is 5.384 deg while the standard deviation is 1.6 deg. As far as the vertical mooring line, the maximum tension is 96.66 N, the minimum tension is 80.96 N and the standard deviation is 2.231 N. Therefore, it is verified that there is no slack condition for the vertical mooring lines.

Computational time

Total computational time is 7 days (168 hours) which consists of CFD (Computational Fluid Dynamics) and BIEM (Boundary Integral Element Method) simulations. Essentially, the whole computational time was taken by the CFD simulation. The CFD simulations for the decay tests in surge and heave take 168 hours per simulation. BIEM method for panchromatic considered sea state simulation only takes 1 min and 53 sec.

Table 2. Comparison of numerical and experimental statistical quantities

	Surge		Heave	
	Exp. (COER)	NAF X=0 Y=1.7	Exp. (COER)	NAF X=0 Y=1.7
Mean (mm)	0	0.1	0	0.3
Std (mm)	37.83	44.11	22.89	24.83
Skewness	0.01775	-0.0023	-0.0155	-0.00524
kurtosis	3.34	3.09	2.76	3.22

It should be noted that after the CFD simulations for the decay tests are finished and the damping coefficients are imported into the WAMIT\SIMO\RIFLEX model, no additional CFD simulation is required for a new sea state. Regarding the CFD simulations, a Linux operating machine with Intel(R) Xeon(R) CPU E5-2687W 0 @ 3.10 GHz processor is used, and for the BIEM simulations a Windows server operating machine with Intel(R) Xeon(R) CPU E5-2650 0 @ 2.00 GHz processor is used.

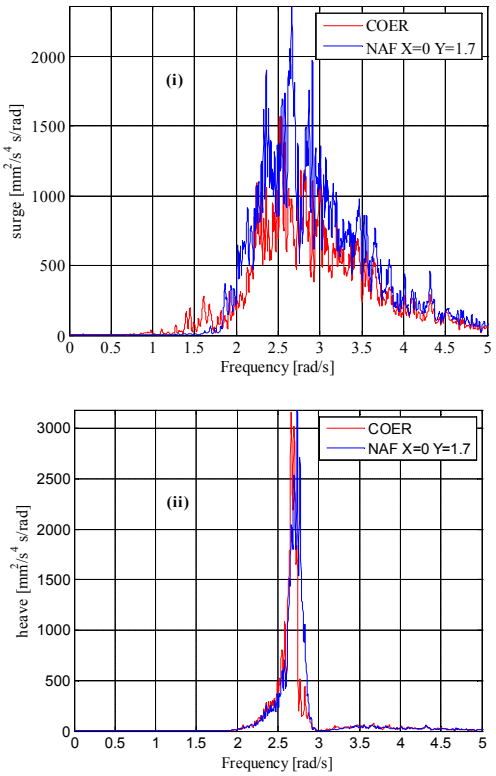

Fig. 13: Comparison of surge and heave spectra for the test panchromatic sea state

CONCLUSIONS

In the present paper, a hybrid Computational Fluid Dynamics (CFD) and Boundary Integral Element Method (BIEM) framework is developed in order to study the response of a moored Multibody Energy Device (MED) to a panchromatic sea state.

The Numerical Analysis Framework (NAF) includes two different models; the first model uses Navier-Stokes equations to describe the flow field and is solved with an in-house CFD code, while the second model uses boundary-integral equation method and is solved with the tool WAMIT\SIMO\RIFLEX. By studying the free decay tests with the Navier-Stokes based model, the uncoupled linear and quadratic damping coefficients of the MED in surge and heave directions are calculated. These coefficients are given as input to the WAMIT\SIMO\RIFLEX model and the responses of the MED to different regular and irregular waves are determined.

Based on the blind competition results, the responses calculated from NAF are in a very good agreement with corresponding experimental data. CFD models in combination with BIEM based models can provide high fidelity numerical tools, while keep the computational time reasonable. Proper estimation of damping coefficients are very important parameter in studying Wave Energy Converts (WECs); the reason is that WECs natural frequencies are very close to ocean wave's peak frequency.

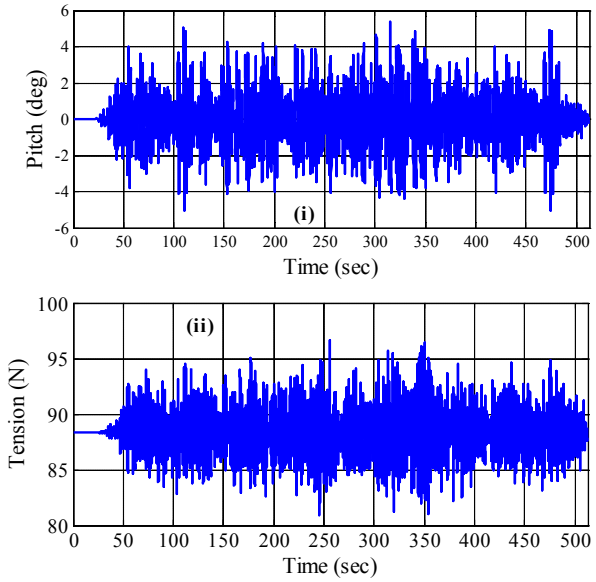

Fig. 14: Time histories of pitch motion of SHCPC (Fig. 13i) and tension of vertical mooring line (Fig. 13 ii)

Finally, it would be interesting to perform a finer grid analysis in CFD model in order to increase the accuracy of damping coefficients, compare the results from NAF with corresponding results with different damping estimation techniques (distributed damping coefficients) and studying the power performance of the presented MED with possible different Power Take-Off configurations.

ACKNOWLEDGMENTS

The authors acknowledge the financial support from the Research Council of Norway granted through the Centre for Ships and Ocean Structures, Norwegian University of Science and Technology as well as COER for organizing the competition and for sharing the model test results after the completion of the competition.

REFERENCES

[1] Agamloh, E. B., Wallace, A. K. and Von Jouanne, A., (2008), "Application of fluid-structure interaction simulation of an ocean wave energy extraction device," Renewable Energy, 33: 748-757

[2] Bhinder M. A, Mingham C. G., Causon D. M, Rahmati M. T, Aggidis G. A, and Chaplin R. V., (2009), "A joint numerical and experimental study of a surging point absorbing wave energy converter (WRASPA)," ASME 28th International Conference on Ocean, Offshore and Arctic Engineering, Honolulu, Hawaii.

[3] Westphalen, J., Greaves, D. M., Raby, A., Hu, Z. Z., Causon, D. M., Mingham, C. G., Omidvar, P., Stansby, P. K., and Rogers B. D., (2014), "Investigation of wave-structure interaction using state of the art CFD techniques", Open Journal of Fluid Dynamics 4: 18-43.

[4] Falnes J, Budal K., (1978), "Wave-power conversion by point absorbers," Norwegian Maritime Research 6(4):2–11.

[5] Mei C. C., Newman J. N., (1980), "Wave power extraction by floating bodies," 1st Symposium on Wave Energy Utilization, Gotenborg, Sweden
[6] Falnes J., (1980), "Radiation impedance matrix and optimum power absorption for interacting oscillators in surface waves," Applied Ocean Research, 2(2):75–80.
[7] Falnes J., (1999), "Wave-energy conversion through relative motion between two single-mode oscillating bodies," Journal of Offshore Mechanics and Arctic Engineering 121:32-38.
[8] Falnes J., (2002), "Ocean waves and oscillating systems," Cambridge University Press
[9] Payne G. S., Taylor J. M., Bruce T, Parkin P., (2008), "Assessment of boundary-element method for modeling a free-floating sloped wave energy device. Part 1: Numerical modeling," Ocean Engineering 38:333–341.
[10] Gomes R, Henriques J, Gato L, Falcão A., (2010), "IPS two-body wave energy converter: acceleration tube optimization", 20th International Offshore and Polar Engineering Conference, Beijing, China.
[11] Michailides C, Angelides D. C., (2015), "Optimization of a flexible floating structure for wave energy production and protection effectiveness," Engineering Structures 85:249-263.
[12] Michailides C, Angelides D. C. (2012) "Modeling of energy extraction and behavior of a Flexible Floating Breakwater," Applied Ocean Research 35:77-94.
[13] Muliawan, M. J., Karimirad, M. and Moan, T., (2013), "Dynamic response and power performance of a combined spar-type floating wind turbine and coaxial floating wave energy converter," Renewable Energy 50:47–57.
[14] Muliawan, M. J., Karimirad, M., Gao, Z. and Moan, T., (2013), "Extreme responses of a combined spar-type floating wind turbine and floating wave energy converter (STC) system with survival modes," Ocean Engineering 65:71–82.
[15] Muliawan, M. J., Gao, Z., Moan, T. and Babarit, A. (2013), "Analysis of a two-body floating wave energy converter with particular focus on the effects of power take-off and mooring systems on energy capture", Journal of Offshore Mechanics and Arctic Engineering, 135(3): 031902.
[16] Michailides, C., Luan, C., Gao, Z. and Moan, T., (2014), "Effect of flap type wave energy converters on the response of a semi-submersible wind turbine in operational conditions," 33rd International Conference on Ocean Offshore and Arctic Engineering, San Francisco, CA
[17] Michailides, C., Gao, Z. and Moan, T., (2014), "Response analysis of the combined wind\wave energy concept SFC in harsh environmental conditions. 1st International Conference on Renewable Energies Offshore, Lisbon, Portugal
[18] DNV (2010) Recommended Practice – Environmental Conditions and Environmental Loads. DNV-RP-C205. Høvik, Norway.
[19] Nematbakhsh A., Olinger, D. J. and Tryggvason, G., (2013), "A nonlinear computational model for floating wind turbines," ASME Journal of Fluids Engineering 135: 121103
[20] Nematbakhsh A., Olinger, D. J. and Tryggvason, G., (2014), "Nonlinear simulation of a spar buoy floating wind turbine under extreme ocean conditions," Journal of Renewable and Sustainable Energy 6:033121.
[21] Nematbakhsh, A., Bachynski, E. E., Gao, Z. and Moan, T., (2014), "Comparison of wave-induced response of a TLP wind turbine obtained by CFD method and potential theory," 24th International Ocean and Polar Engineering Conference, Busan, Korea.
[22] Costello, R., Padeletti, D., Davidson, J. and Ringwood, J.V., (2014), "Comparison of numerical simulations with experimental measurements for the response of a modified submerged horizontal cylinder moored in waves", 33rd International Conference on Ocean Offshore and Arctic Engineering, San Francisco, CA
[23] Osher S., Sethian J. A., (1988), "Fronts propagating with curvature-dependent speed: algorithms based on Hamilton-Jacobi formulations", Journal of Computational Physics **79**: 12–49.
[24] Mittal, R. and Iaccarino, G., (2005), "Immersed boundary methods", Annual Review of Fluid Mechanics, **37**: 239-261.
[25] WAMIT (2009) User Manual – program version 6.4. WAMIT, Inc. (www.wamit.com).
[26] MARINTEK (2011) SIMO User's Manual. Trondheim, Norway.
[27] MARINTEK (2013) RIFLEX User's Manual. Trondheim, Norway.
[28] Faltinsen, O. (1993), "Sea loads on ships and offshore structures," Cambridge University Press.

